ELSEVIER

www.elsevier.nl/locate/jelechem

Journal of Electroanalytical Chemistry 481 (2000) 13–23

Journal of Electroanalytical Chemistry

Effects of temperature on hydrogen absorption into palladium hydride electrodes in the hydrogen evolution reaction

Wu-Shou Zhang [a,b,*], Zhong-Liang Zhang [a], Xin-Wei Zhang [b]

[a] *Institute of Chemistry, Chinese Academy of Sciences, PO Box 2709, Beijing 100080, PR China*
[b] *Institute of Applied Physics and Computational Mathematics, PO Box 8009, Beijing 100088, PR China*

Received 20 September 1999; received in revised form 15 November 1999; accepted 16 November 1999

Abstract

On the basis of the Volmer–Tafel route of the hydrogen evolution reaction, and thermokinetic considerations involving H–H interactions and stress fields of hydrogen in β-PdH_x, we discuss the analytical and numerical effects of temperature on the loading ratio, charging rate and self-stress for hydrogen absorption into electrodes of β-phase PdH_x under galvanostatic and potentiostatic charging conditions. It was found that changes in the loading ratio, overpotential and current density with temperature can be expressed in terms of four parameters, i.e. enthalpies of adsorption and absorption of hydrogen on (into) palladium, and apparent activation energies of exchange current density of the Volmer and Tafel reactions, in addition to the usual physical quantities such as temperature and overpotential etc., although more factors are involved in the actual process. With increasing temperature, the absorption process tends to be determined by the surface reaction and the self-stresses decrease under the galvanostatic charging condition; however, the absorption time decreases but the self-stresses change slightly for the potentiostatic charging. Finally, our theory is consistent with the available experimental results.

Keywords: Pd|H electrode; Hydrogen evolution reaction; Temperature; Activation energy; Stress; Diffusion

1. Introduction

In the past few years, some experiments have been carried out on the effects of temperature on the loading ratio and kinetics of hydrogen absorption into palladium electrodes in the hydrogen evolution reaction (her) [1–5]. Bernardini et al. [5] have found that the atomic ratio of H to Pd, n_H, decreases with temperature by a slope of $\partial n_H/\partial T \sim -1.6\times10^{-3}$ K^{-1} under the galvanostatic charging condition, and $\partial n_H/\partial T \sim -8.7\times10^{-4}$ K^{-1} under the potentiostatic charging condition with H_3PO_4 electrolyte and a temperature range 25 to 175°C. As concerns the kinetics of the Pd|H electrode, Riley et al. observed that the absorption time decreases with increasing temperature [1]. Another related problem is that some experiments are carried out at scattered temperatures around the ambient temperature [6–8], hence for the quantitative comparison between different results a temperature correction must be taken into account. Although these temperature effects can be explained qualitatively by the thermodynamics of the Pd + H system [9,10] and the kinetics of the her [11], there has been no quantitative analysis up to now. In this paper, we will deal with this subject based on the Volmer–Tafel route of the her and the kinetics of the Pd|H electrode [9–14]. As was done in earlier papers [13,14], we discuss only the behaviour of the β-phase PdH_x, although our theory can be extended to the solid solution situation.

2. Model

Consider hydrogen absorption into a PdH_x plate electrode in the her (see Fig. 1). The plate thickness $2L$ is small compared with the length and width ($x-y$ plane), which allows our analysis to be reduced to a one-dimensional problem. The hydrogen atoms are absorbed symmetrically by both sides; this central symmetry simplifies our discussion and only a half space needs to be considered.

* Corresponding author. Fax: +86-10-62559373.
E-mail address: wszhang@a-1.net.cn (W.-S. Zhang)

0022-0728/00/$ - see front matter
PII: S0022-0728(99)00472-6

At the outer surface there are three steps, i.e. the Volmer, Tafel and penetration reactions, taking place in the her at the same time [11,13]. The rates of the Volmer, Tafel and penetration steps are:

$$j_{\mathrm{V}} = r\Gamma_{\mathrm{s}}F \left\{ \begin{array}{c} A_{+\mathrm{V}}a_{\mathrm{R}}\theta \exp\left(-\dfrac{U_{+\mathrm{V}}}{RT}+\dfrac{U_{\mathrm{s}}\theta}{2RT}+\dfrac{\beta_{\mathrm{V}}FE}{RT}\right) \\ -A_{-\mathrm{V}}a_{\mathrm{O}}(1-\theta)\exp\left(-\dfrac{U_{-\mathrm{V}}}{RT}-\dfrac{U_{\mathrm{s}}\theta}{2RT}-\dfrac{(1-\beta_{\mathrm{V}})FE}{RT}\right) \end{array} \right\} \quad (1)$$

$$j_{\mathrm{T}} = 2r^2\Gamma_{\mathrm{s}}^2F\left\{A_{+\mathrm{T}}a_{\mathrm{H}_2}(1-\theta)^2\exp\left(-\frac{U_{+\mathrm{T}}}{RT}-\frac{U_{\mathrm{s}}\theta}{RT}\right) - A_{-\mathrm{T}}\theta^2\exp\left(-\frac{U_{-\mathrm{T}}}{RT}+\frac{U_{\mathrm{s}}\theta}{RT}\right)\right\} \quad (2)$$

and

$$j_{\mathrm{P}} = r\Gamma_{\mathrm{s}}\Gamma_{\mathrm{b}}F \left\{ \begin{array}{c} A_{+\mathrm{P}}(1-\theta)n_{\mathrm{H}}\exp\left(-\dfrac{U_{+\mathrm{P}}}{RT}-\dfrac{U_{\mathrm{s}}\theta}{2RT}+\dfrac{U_{\mathrm{b}}n_{\mathrm{H}}}{2RT}-\dfrac{V_{\mathrm{H}}\sigma}{2RT}\right) \\ -A_{-\mathrm{P}}\theta(1-n_{\mathrm{H}})\exp\left(-\dfrac{U_{-\mathrm{P}}}{RT}+\dfrac{U_{\mathrm{s}}\theta}{2RT}-\dfrac{U_{\mathrm{b}}n_{\mathrm{H}}}{2RT}+\dfrac{V_{\mathrm{H}}\sigma}{2RT}\right) \end{array} \right\} \quad z=0 \quad (3)$$

respectively. In the electrolyte solution, the dissolved H_2 molecules that are produced in the Tafel reaction congregate to H_2 gas bubbles and escape to the gas phase above the liquid level. We call this the congregation reaction and its rate can be expressed as:

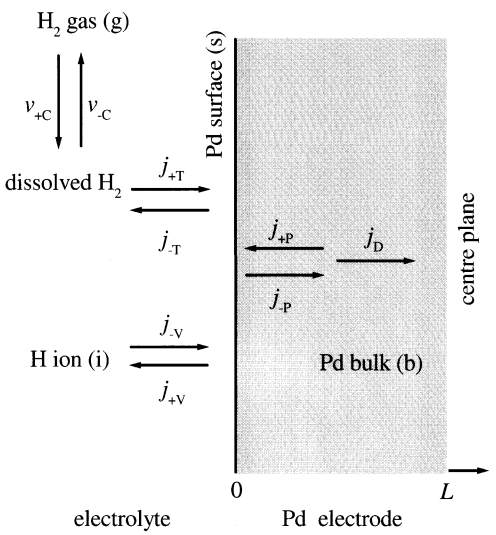

Fig. 1. Schematic representation of various steps in the process of hydrogen absorption into a Pd plate electrode in the hydrogen evolution reaction. In the figure, only a half space is presented due to the central symmetry property of this system.

$$v_{\mathrm{C}} = A_{+\mathrm{C}}f_{\mathrm{H}_2}\exp\left(-\frac{U_{+\mathrm{C}}}{RT}\right) - A_{-\mathrm{C}}a_{\mathrm{H}_2}\exp\left(-\frac{U_{-\mathrm{C}}}{RT}\right) \quad (4)$$

In Eqs. (1)–(4), A_i is the Arrhenius frequency factor of the rate constant for reaction i; E is the electrode potential; U_i is the activation energy of reaction i; U_{b} is the non-ideal interaction energy of H in the bulk of β-PdH_x, $U_{\mathrm{b}} = 44.9$ kJ mol^{-1} for both H and D [15,16]; U_{s} is the heterogeneity energy of the Frumkin adsorption, its value depends on the additives in the electrolyte and pH; V_{H} is the partial molar volume of H in β-PdH_x, $V_{\mathrm{H}} = 1.55$ cm^3 mol^{-1} [14,17,18]; a_i is the activity of substance i dissolved in the electrolyte solution; f_{H_2} is the fugacity of the H_2 gas; j_i is the current density (cd) of reaction i; n_{H} is the H/Pd atomic ratio; r is the surface roughness factor; v_{C} is the reaction rate of the H_2 congregation reaction; $\Gamma_{\mathrm{b}} = 0.10$ mol cm^{-3}, the maximum molar number of available sites for H per unit volume of PdH_x (expansion effect due to H insertion is concerned [19]); $\Gamma_{\mathrm{s}} = 2.20\times10^{-9}$ mol H cm^{-2} [20], is the maximum molar number of available sites for H per real unit area; β_{V} is the transfer coefficient of the Volmer reaction; θ is the fractional surface coverage of H on Pd; σ is the self-stress and an expression for it will be given below. The other symbols have their usual meanings.

In Eqs. (1)–(4), the subscripts V, T, P and C denote the Volmer, Tafel, penetration and congregation reactions, respectively; O and R = H_3^+O and H_2O, respectively, in acidic solution and at low negative overpotential; otherwise, O and R = H_2O and OH^-, respectively, in basic solution or at high negative overpotential; + and − represent the anodic and cathodic reactions, respectively.

For simplicity, we choose all of the symmetry factors to be 1/2 in Eqs. (1)–(3). The transfer coefficient β_{V} is almost a constant and does not vary with temperature at low overpotentials [21], and it changes with T at a rate of -1.3×10^{-3} K^{-1} at high overpotential [22]. We will assume $\beta_{\mathrm{V}} = 1/2$ and that it does not change with temperature or overpotential. Because our attention is focused on the aspects of hydrogen absorption into the electrode, all of the solute activities will be assumed as constant although they actually change with T [23,24] for constant molality concentrations of solute. On the other hand, although there is no charge transfer in the Tafel and penetration reactions, we still express the reaction rate as a cd for comparison.

The self-stress σ in Eq. (3) has the form [14,25,26]:

$$\sigma = -\frac{2V_{\mathrm{H}}Y\Gamma_{\mathrm{b}}}{3(1-\nu)}\left(\Delta n_{\mathrm{H}} - \frac{1}{L}\int_0^L \Delta n_{\mathrm{H}}\mathrm{d}z\right) \quad (5)$$

where Y is Young's modulus of Pd, $Y = 1.16\times10^{11}$ Pa [27]; $\nu = 0.39$, Poisson's ratio; $\Delta n_{\mathrm{H}} = n_{\mathrm{H}} - n_{\mathrm{H},0}$, $n_{\mathrm{H},0}$ is the homogeneous initial value of n_{H} in β-PdH_x.

Taking account of the mass balance on the Pd surface, we obtain the time dependence of the adsorbed hydrogen coverage:

$$\frac{\mathrm{d}\theta}{\mathrm{d}t}=\frac{1}{r\Gamma_s F}(j_T+j_P-j_V) \tag{6}$$

In the bulk of the β-PdH_x electrode, the diffusion flow of hydrogen has the form:

$$j_D=-\Gamma_b F A_D \exp\left(-\frac{U_D}{RT}\right)\times\left[1+\left(\frac{U_b}{RT}+\frac{2}{3}\frac{V_H^2 Y\Gamma_b}{RT}\right)n_H(1-n_H)\right]\frac{\partial n_H}{\partial z} \tag{7}$$

where A_D, the pre-exponential factor of the diffusion coefficient, is 0.0113 and 0.0105 $cm^2\ s^{-1}$ for H and D, respectively; U_D, the activation energy for H diffusion, is 27.1 and 25.9 kJ mol^{-1} for H and D, respectively [28,29]. Formulation of the starting equation for calculation of the time-space dependence of n_H requires the introduction of the flow equation into the mass balance equation, Fick's second law [30]:

$$\frac{\partial n_H}{\partial t}=-\frac{1}{\Gamma_b F}\nabla\cdot j_D \tag{8}$$

The inner surface boundary condition is the zero flux of hydrogen, i.e. $j_D=0$:

$$\frac{\partial n_H}{\partial z}=0,\ z=L \tag{9}$$

At the outer surface:

$$j_D=-j_P,\ z=0 \tag{10}$$

This equation couples the surface reactions with the bulk process.

Eqs. (1)–(8) with the boundary conditions of Eqs. (9) and (10) form the basis for all consequent and exact treatments of hydrogen absorption involving temperature and self-stresses. These equations can be solved numerically using, e.g. the method described earlier [14].

3. Results

In this section, we will discuss various effects of temperature on hydrogen absorption into palladium hydride electrodes for the topics of equilibrium state, steady-state, absorption kinetics and diffusion induced stress successively. Although our model is established for plate shaped electrodes, the results of equilibrium and steady states are shape independent.

3.1. Equilibrium state

Prior to detailed discussion of the situation of the her, we focused on the equilibrium state. To be specific, the electrode reaction is confined to the normal condition of $f_{H_2}=1$ atm and $0°C\le T\le 100°C$. The first assumption means that the partial pressure of hydrogen is equal to ambient, which can be accomplished by carrying out the experiment under a H_2 gas atmosphere or blowing hydrogen gas from the bottom of the cell. Although many experiments are employed without the blowing of H_2 gas and the initial state differs from this equilibrium state, the hydrogen bubbles produced in the her makes the H partial pressure approximately equal to 1 atm, hence the corresponding equilibrium state is the same as that in a hydrogen atmosphere. These choices of pressure and temperature ensure the Pd + H system is in the β-phase in equilibrium or in the her.

If the equilibrium case is considered where the net flux becomes zero, from Eq. (1) we obtain:

$$\frac{\theta_0}{1-\theta_0}\exp\left(\frac{U_s\theta_0}{RT}\right)=\frac{a_O}{a_R}\exp\left(-\frac{\Delta S_{si}}{R}+\frac{\Delta H_{si}}{RT}\right)\exp\left(-\frac{FE_0}{RT}\right) \tag{11}$$

with

$$\begin{cases}\Delta S_{si}=R\ln\left(\dfrac{A_{+V}}{A_{-V}}\right)\\ \Delta H_{si}=U_{+V}-U_{-V}\end{cases} \tag{12}$$

Combining Eqs. (2) and (4) gives:

$$f_{H_2}^{1/2}=\exp\left(-\frac{\Delta S_{gs}}{R}+\frac{\Delta H_{gs}}{RT}\right)\frac{\theta_0}{1-\theta_0}\exp\left(\frac{U_s\theta_0}{RT}\right) \tag{13}$$

with

$$\begin{cases}\Delta S_{gs}=\dfrac{R}{2}\ln\left(\dfrac{A_{+T}A_{+C}}{A_{-T}A_{-C}}\right)\\ \Delta H_{gs}=(U_{+T}-U_{-T}+U_{+C}-U_{-C})/2\end{cases} \tag{14}$$

In Eqs. (11)–(14) and the discussion below, ΔS_{ij} and ΔH_{ij} represent entropy and enthalpy changes from ideal state i to ideal state j (dilute solution, no H–H interaction being concerned), respectively. Subscripts b, g, i and s represent hydrogen in Pd bulk, H_2 gas, ionic state (H_3^+O or H_2O) and surface adsorption state, respectively. Of course, $\Delta S_{ij}=-\Delta S_{ji}$ and $\Delta H_{ij}=-\Delta H_{ji}$. θ_0 is the equilibrium surface coverage and E_0 is the equilibrium electrode potential. Eqs. (11) and (13) describe the electrochemical and chemical adsorption isotherms of H on Pd, respectively [11,20,31].

Combining Eqs. (11) and (13) gives:

$$f_{H_2}^{1/2}=\frac{a_O}{a_R}\exp\left(-\frac{\Delta S_{gi}}{R}+\frac{\Delta H_{gi}}{RT}\right)\exp\left(-\frac{FE_0}{RT}\right) \tag{15}$$

with

$$\begin{cases} \Delta S_{gi} = \Delta S_{gs} + \Delta S_{si} \\ \Delta H_{gi} = \Delta H_{gs} + \Delta H_{si} \end{cases} \quad (16)$$

Because the reversible electrode potential E_0 is determined by the hydrogen pressure, temperature and solute concentration (or pH value), ΔS_{gi} and ΔH_{gi} must be constant if these parameters are fixed although the electrochemical and chemical adsorption parameters may be modified by electrode surface properties. This equation is another form for the potential of the reversible hydrogen electrode (RHE) as a function of the hydrogen pressure, temperature and pH value. We can obtain the change of equilibrium potential with temperature from Eq. (15):

$$\frac{\partial E_0}{\partial T} = \frac{1}{FT}(FE_0 - \Delta H_{gi}) \quad (17)$$

At the same time we can obtain exchange cds (per real unit area) as functions of T. Contrary to ones expectation, it is the weak adsorption, not the strong adsorption, that dominates the H absorption into the β-PdH_x electrode, as has been verified experimentally and theoretically [11–13,21,32]. Therefore, the Frumkin adsorption reduces to the Langmuir type with $U_s\theta_0 \to 0$ and $1-\theta_0 \to 1$. Eliminating E_0 between Eqs. (1) and (15) gives the exchange cd of the Volmer step:

$$j_{0V} = \Gamma_s F(A_{+V}A_{-V}a_O a_R)^{1/2}\left(\frac{A_{+T}}{A_{-T}}\frac{A_{+C}}{A_{-C}}f_{H_2}\right)^{1/4} \times \exp\left(-\frac{U_{0V}}{RT}\right) \quad (18)$$

with

$$U_{0V} = \Delta H_{gi}/2 + U_{-V} \quad (19)$$

and eliminating a_{H_2} between Eqs. (2) and (4) gives the exchange cd of the Tafel step:

$$j_{0T} = 2\Gamma_S^2 F A_{+T} f_{H_2}\frac{A_{+C}}{A_{-C}}\exp\left(-\frac{U_{0T}}{RT}\right) \quad (20)$$

with

$$U_{0T} = 2\Delta H_{gs} + U_{-T} \quad (21)$$

where the measurable quantities, U_{0V} and U_{0T} are apparent activation energies of j_{0V} and j_{0T}, respectively. It was observed that $U_{0V} = 25$–33 and $U_{0T} = 27$ kJ mol^{-1} in 0.5–1 M H_2SO_4 [21,22].

Eqs. (11)–(21) describe the equilibrium processes at the outer surface of the Pd electrode; the remaining processes are associated with the hydrogen absorption into the electrode. Eq. (3) in equilibrium gives:

$$\frac{\theta_0}{1-\theta_0}\exp\left(\frac{U_s\theta_0}{RT}\right) = \exp\left(-\frac{\Delta S_{sb}}{R} + \frac{\Delta H_{sb}}{RT}\right)\frac{n_H}{1-n_H}\exp\left(\frac{U_b n_H}{RT}\right) \quad (22)$$

with

$$\begin{cases} \Delta S_{sb} = R\ln\left(\frac{A_{-P}}{A_{+P}}\right) \\ \Delta H_{sb} = U_{-P} - U_{+P} \end{cases} \quad (23)$$

The subscript sb represents the state transformation from the surface adsorption to the bulk absorption. It is easy to obtain the relationship between potential and the loading ratio using Eqs. (11) and (22):

$$\exp\left(-\frac{FE_0}{RT}\right) = \frac{a_R}{a_O}\exp\left(-\frac{\Delta S_{ib}}{R} + \frac{\Delta H_{ib}}{RT}\right)\frac{n_H}{1-n_H}\exp\left(\frac{U_b n_H}{RT}\right) \quad (24)$$

with

$$\begin{cases} \Delta S_{ib} = \Delta S_{is} + \Delta S_{sb} \\ \Delta H_{ib} = \Delta S_{is} + \Delta H_{sb} \end{cases} \quad (25)$$

In addition, eliminating θ_0 between Eqs. (13) and (22) gives:

$$f_{H_2}^{1/2} = \exp\left(-\frac{\Delta S_{gb}}{R} + \frac{\Delta H_{gb}}{RT}\right)\frac{n_H}{1-n_H}\exp\left(\frac{U_b n_H}{RT}\right) \quad (26)$$

with

$$\begin{cases} \Delta S_{gb} = \Delta S_{gs} + \Delta S_{sb} \\ \Delta H_{gb} = \Delta H_{gs} + \Delta H_{sb} \end{cases} \quad (27)$$

Eq. (26) is exactly the isotherm of H absorption into β-PdH_x; it was found that $\Delta S_{gb} = -53.5$ and -53.1 J mol^{-1} K^{-1}, and $\Delta H_{gb} = -50.1$ and -47.7 kJ mol^{-1} for H and D, respectively; $U_b = 44.9$ kJ mol^{-1} for both H and D [15,16]. Although changes in entropy and enthalpy in each step may be influenced by the Pd surface property or solution composition, their sums must be constant values as indicated by Eq. (27). The loading ratio change with temperature under a fixed pressure is:

$$\frac{\partial n_H}{\partial T} = \frac{\Delta H_{gb} + U_b n_H}{RT^2\left(\frac{1}{n_H(1-n_H)} + \frac{U_b}{RT}\right)} \quad (28)$$

which is -1.0×10^{-3} K^{-1} in Fig. 2(a), the curve $j = 0$. This curve is the isobar of H absorption into β-PdH_x under 1 atm pressure.

The above formulae except Eqs. (18)–(21) can be extended to the situation of the α-phase with some parameters adjusted when the hydrogen pressure is low or the temperature is high enough. Because the strong adsorption is the precursor for α-phase absorption, the

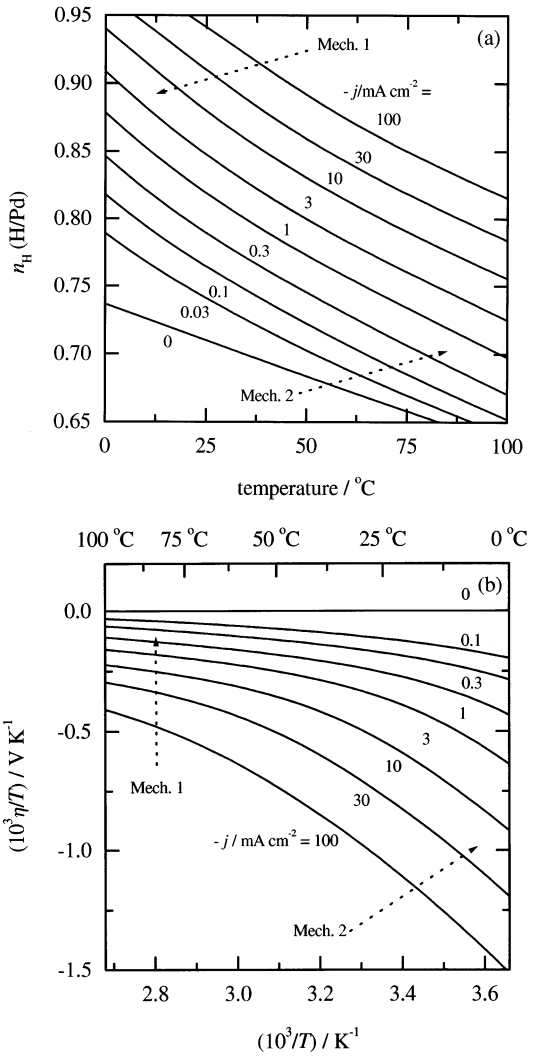

Fig. 2. Effects of temperature on (a) the loading ratio and (b) the overpotential for H absorption into a β-phase Pd|H electrode under galvanostatic charging conditions. Current densities are shown beside each curve. Mech. 1 and Mech. 2 represent the fast Volmer–slow Tafel mechanism and coupled Volmer–Tafel mechanism, respectively. The parameters: $A_{+V}a_R = 4.13 \times 10^8$ s^{-1}, $A_{-V}a_O = 1.60 \times 10^{11}$ s^{-1}, $A_{+T}A_{+C}/A_{-C} = 6.24 \times 10^{11}$ cm^2 atm^{-1} mol^{-1} s^{-1}, $A_{-T} = 3.51 \times 10^{25}$ cm^2 mol^{-1} s^{-1}, $A_{+P} = 1.25 \times 10^8$ cm^3 mol^{-1} s^{-1}, $A_{-P} = 1.58 \times 10^{12}$ cm^3 mol^{-1} s^{-1}; $U_{+V} = 94$, $U_{-V} = 0$, $U_{+T} + U_{+C} - U_{-C} = 27$, $U_{-T} = 83$, $U_{+P} = 42$, $U_{-P} = 20$, $U_s = 15$ kJ mol^{-1}; $r = 1$, $f_{H_2} = 1$ atm.

exchange cds and the corresponding activation energies have other forms. Two different types of surface state, strong adsorption for the α-phase and weak adsorption for the β-phase, play key roles in different ranges of chemical potential and they jointly make the Pd function as a good catalyst. For the situation of the α + β mixed phase, the potential does not change with the hydrogen loading ratio and it must be treated by other methods such as those discussed in Ref. [33].

3.2. Steady-state hydrogen absorption

In the steady-state, the hydrogen produced in the Volmer step is removed uniquely by the Tafel reaction, i.e. $j = j_V = j_T$; the self-stress disappears and the penetration reaction reaches equilibrium. Like Eq. (22), we may write:

$$\frac{\theta}{1-\theta}\exp\left(\frac{U_s\theta}{RT}\right) = \exp\left(-\frac{\Delta S_{sb}}{R} + \frac{\Delta H_{sb}}{RT}\right)\frac{n_H}{1-n_H}\exp\left(\frac{U_b n_H}{RT}\right) \quad (29)$$

At the same time, we suppose the congregation reaction to be in equilibrium in each case. Because there are two mechanisms of the her, i.e. the fast Volmer–slow Tafel type at low cd in acidic solution and the coupled Volmer–Tafel type in basic solution or at high cd in acidic solution, taking place on the Pd electrode, we will discuss the steady-state absorption in these two situations successively.

3.2.1. Fast Volmer–slow Tafel mechanism

In this case, the Tafel step is irreversible but the Volmer reaction is in pseudo-equilibrium. Like Eqs. (11) and (24), we obtain

$$\frac{\theta}{1-\theta}\exp\left(\frac{U_s\theta}{RT}\right) = \frac{a_O}{a_R}\exp\left(-\frac{\Delta S_{si}}{R} + \frac{\Delta H_{si}}{RT}\right)\exp\left(-\frac{FE}{RT}\right) \quad (30)$$

and

$$\exp\left(-\frac{FE}{RT}\right) = \frac{a_R}{a_O}\exp\left(-\frac{\Delta S_{ib}}{R} + \frac{\Delta H_{ib}}{RT}\right)\frac{n_H}{1-n_H}\exp\left(\frac{U_b n_H}{RT}\right) \quad (31)$$

Because the overpotential is low, the value of θ is small and the adsorption can be simplified to the Langmuir type as in the discussion about j_{0V} and j_{0T}. Introducing Eq. (30) into Eq. (2), we have:

$$j = -j_{-T} = -2r^2\Gamma_s^2 F A_{-T}\left(\frac{A_{-V}a_O}{A_{+V}a_R}\right)^2 \times \exp\left(-\frac{2FE - 2\Delta H_{si} + U_{-T}}{RT}\right) \quad (32)$$

This polarisation relation gives the well known Tafel slope of $RT/2F$. Similarly, substituting Eq. (29) into Eq. (2) gives:

$$j = -j_{-T} = -2r^2\Gamma_s^2 F A_{-T}\left(\frac{A_{+P}}{A_{-P}}\right)^2\left(\frac{n_H}{1-n_H}\right)^2 \times \exp\left(\frac{2\Delta H_{sb} + 2U_b n_H - U_{-T}}{RT}\right) \quad (33)$$

which describes n_H as a function of j.

For galvanostatic charging, we obtain the loading ratio change with temperature using Eq. (33):

$$\frac{\partial n_H}{\partial T} = \frac{\Delta H_{gb} + U_b n_H - U_{0T}/2}{RT^2\left(\frac{1}{n_H(1-n_H)} + \frac{U_b}{RT}\right)} \tag{34}$$

which is -1.2×10^{-3} K^{-1} in Fig. 2(a). From Eq. (32), we obtain the change of potential with temperature:

$$\frac{\partial E}{\partial T} = \frac{1}{FT}(FE - \Delta H_{si} + U_{-T}/2) \tag{35}$$

The overpotential, $\eta = E - E_0$, change with temperature can be obtained by combining this equation with Eq. (17):

$$\frac{\partial \eta}{\partial T} = \frac{1}{FT}(F\eta + U_{0T}/2) \tag{36}$$

It can be expressed by a more compact form:

$$\frac{\partial(\eta/T)}{\partial(1/T)} = -\frac{U_{0T}}{2F} \tag{37}$$

which is -0.14 V in Fig. 2(b).

For potentiostatic charging (η = constant), the loading ratio change with temperature can be obtained by combining Eqs. (17) and (31):

$$\frac{\partial n_H}{\partial T} = \frac{\Delta H_{gb} - \Delta H_{gs} + U_b n_H + F\eta}{RT^2\left(\frac{1}{n_H(1-n_H)} + \frac{U_b}{RT}\right)} \tag{38}$$

which is -9.1×10^{-4} K^{-1} in Fig. 3(a). Because this her mechanism is valid while the value of η is very small, the contribution of $F\eta$ can be omitted in this equation. By comparing Eq. (38) with Eq. (28), we find the loading ratio decreases somewhat more slowly than in the equilibrium case because an additional positive numerator $-\Delta H_{gs}$ appears in Eq. (38). The cd change with temperature can be obtained by combining Eqs. (17) and (32):

$$\frac{\partial \ln(-j)}{\partial T} = \frac{U_{0T} + 2F\eta}{RT^2} \tag{39}$$

or

$$\frac{\partial \log(-j)}{\partial(1/T)} = -0.4343\frac{U_{0T}}{R} \tag{40}$$

which is -1.4×10^3 K in Fig. 3(b). In this equation, the term $2F\eta$ is omitted as it is much less than U_{0T}.

3.2.2. Coupled Volmer–Tafel mechanism

When the her is far from equilibrium, $-E \gg RT/F$ and both the Volmer and Tafel steps are completely irreversible. The adsorption follows the Frumkin type at intermediate surface coverage; this means the exponential term is prominent in the hydrogen adsorption isotherm. Eliminating the factor $\exp(U_s\theta/RT)$ between Eqs. (1) and (2) gives:

$$\begin{aligned} j &= -j_{-T} = -j_{-V} = -(j_{-T}j^2_{-V})^{1/3} \\ &= -(2r^4\Gamma_s^4F^3A^2_{-V}A_{-T}a_O^2\theta^2(1-\theta)^2)^{1/3} \\ &\quad \times \exp\left(-\frac{FE + 2U_{-V} + U_{-T}}{3RT}\right) \end{aligned} \tag{41}$$

This equation gives a Tafel slope of $3RT/F$ as discussed earlier [11,34]. At the same time, eliminating $\exp(U_s\theta/RT)$ between Eqs. (2) and (29) gives:

$$\begin{aligned} j &= -j_{-T} = -2r^2\Gamma_s^2F\theta(1-\theta) \\ &\quad \times A_{-T}\frac{A_{+P}}{A_{-P}}\frac{n_H}{1-n_H}\exp\left(\frac{\Delta H_{sb} + U_b n_H - U_{-T}}{RT}\right) \end{aligned} \tag{42}$$

This equation describes the relation between j and n_H.

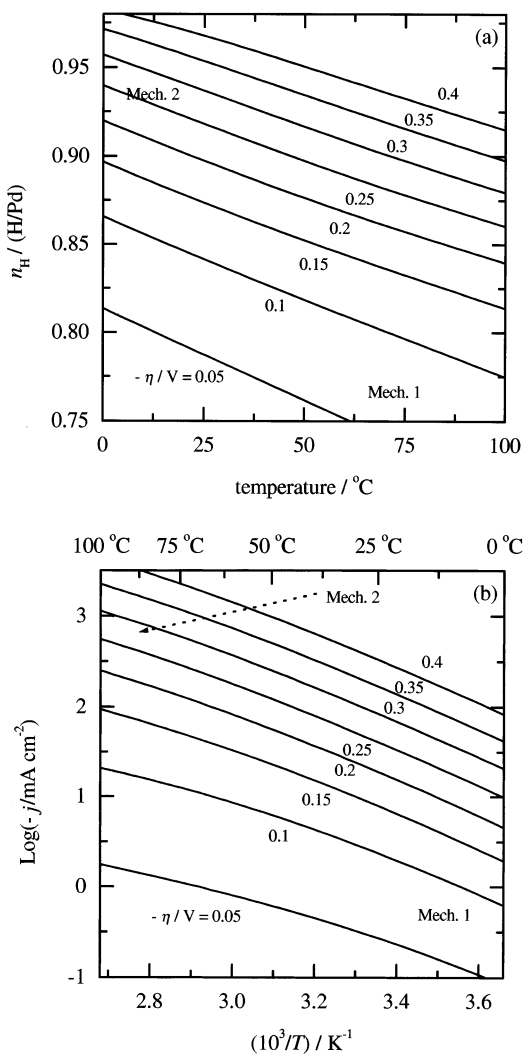

Fig. 3. Effects of temperature on (a) the loading ratio and (b) the current density for H absorption into a β-phase Pd|H electrode under potentiostatic charging conditions. Overpotentials are shown beside each curve. Mech. 1 and Mech. 2 represent the fast Volmer–slow Tafel mechanism and coupled Volmer–Tafel mechanism, respectively. The other parameters are the same as those of Fig. 2.

From the equality of $j_{-V} = j_{-T}$, we have:

$$\sqrt{\theta(1-\theta)}\left[\frac{\theta}{1-\theta}\exp\left(\frac{U_s\theta}{RT}\right)\right]^{3/2} = \frac{A_{-V}a_O}{2r\Gamma_S A_{-T}}\exp\left(\frac{U_{-T}-U_{-V}}{RT}-\frac{FE}{2RT}\right) \quad (43)$$

Combining this equation with Eq. (29) gives:

$$[\theta(1-\theta)]^{1/3}\frac{n_H}{1-n_H}\exp\left(\frac{U_b n_H}{RT}\right) = \left(\frac{A_{-V}a_O}{2r\Gamma_S A_{-T}}\right)^{2/3} \times \frac{A_{-P}}{A_{+P}}\exp\left(-\frac{3\Delta H_{sb}+2U_{-V}-2U_{-T}+FE}{3RT}\right) \quad (44)$$

which describes n_H as a function of E.

For galvanostatic charging, j in Eq. (42) is constant. The partial derivative of the logarithm of Eq. (42) with respect to T gives:

$$\frac{\partial n_H}{\partial T} = \frac{\Delta H_{gb}+\Delta H_{gs}+U_b n_H - U_{0T}}{RT^2\left(\frac{1}{n_H(1-n_H)}+\frac{U_b}{RT}\right)} \quad (45)$$

which is -2.4×10^{-3} K^{-1} in Fig. 2(a). In the deduction, the contribution originating from the term $\theta(1-\theta)$ is omitted as it is a slowly varying quantity. Similarly, we obtain the potential change with T by Eq. (41):

$$\frac{\partial E}{\partial T} = \frac{FE+2U_{-V}+U_{-T}}{FT} \quad (46)$$

Combining this equation with Eq. (17), we obtain the change of overpotential, $\eta = E - E_0$, with temperature:

$$\frac{\partial \eta}{\partial T} = \frac{1}{FT}(F\eta+2U_{0V}+U_{0T}-2\Delta H_{gs}) \quad (47)$$

or

$$\frac{\partial(\eta/T)}{\partial(1/T)} = -\frac{1}{F}(2U_{0V}+U_{0T}-2\Delta H_{gs}) \quad (48)$$

which is -1.5 V in Fig. 2(b).

For potentiostatic charging (η = constant), combining Eqs. (17) and (44) gives the loading ratio change with temperature:

$$\frac{\partial n_H}{\partial T} = \frac{\Delta H_{gb}+U_b n_H+(\Delta H_{gs}+2U_{0V}-2U_{0T}+F\eta)/3}{RT^2\left(\frac{1}{n_H(1-n_H)}+\frac{U_b}{RT}\right)} \quad (49)$$

which is -7.4×10^{-4} K^{-1} in Fig. 3(a). Changes of cd with temperature can be obtained from Eqs. (17) and (41):

$$\frac{\partial \ln(-j)}{\partial T} = \frac{2U_{0V}+U_{0T}-2\Delta H_{gs}+F\eta}{3RT^2} \quad (50)$$

or

$$\frac{\partial \log(-j)}{\partial(1/T)} = -0.4343\frac{2U_{0V}+U_{0T}-2\Delta H_{gs}+F\eta}{3R} \quad (51)$$

which is -2.1×10^3 K in Fig. 3(b).

Figs. 2 and 3 show changes of n_H, η and j with T based on Eqs. (1)–(4) under galvanostatic and potentiostatic charging conditions, respectively. The related parameters, noted in the caption of Fig. 2, result in $\theta_0 = 0.01$, $j_{0V} = 1$ mA cm^{-2}, $j_{0T} = 0.01$ mA cm^{-2} and $j_{0P} = 100$ mA cm^{-2} at 298.15 K. These choices ensure that the adsorption in equilibrium is weak; the her follows the fast Volmer–slow Tafel mechanism, while $-j \le 1$ mA cm^{-2}, or the coupled Volmer–Tafel mechanism, while $-j \gg 1$ mA cm^{-2}, around the ambient temperature; and the penetration reaction is in pseudo-equilibrium in the her. The activation energies are chosen to ensure that $U_{0V} = 33$ kJ mol^{-1}, $U_{0T} = 27$ kJ mol^{-1} and $\Delta H_{gb} = -50$ kJ mol^{-1} as observed experimentally [15,21,22]. All of these parameters are adjusted to simulate the her in the aqueous acidic solution under the ambient pressure, although our method and conclusion are beyond this confinement.

For the situation of galvanostatic charging shown in Fig. 2, we find the amplitude of $\partial n_H/\partial T$ increases with increasing cd and/or decreasing temperature. The dependence of $\partial n_H/\partial T$ on T is easy to understand using Eqs. (28), (34) and (45), in which the amplitude of $\partial n_H/\partial T$ is inversely proportional to T. As far as the effect of cd is concerned, we find the her changes from the equilibrium state to the fast Volmer–slow Tafel mechanism and up to the coupled Volmer–Tafel mechanism with increasing cd, and the corresponding $\partial n_H/\partial T$ is expressed by Eqs. (28), (34) and (45), respectively. Because the terms $\Delta H_{gb}+U_b n_H$, ΔH_{gs} and U_{0T} in the numerators have the same sign (<0), so the increase of $|\partial n_H/\partial T|$ with cd is obvious. As concerns the overpotential, we find that the slopes shown in Fig. 2(b) decline significantly when the mechanism of her changes from the fast Volmer–slow Tafel type to the coupled Volmer–Tafel type (j increases or T decreases), as indicated by Eqs. (37) and (48). At the same time, this result indicates that the amplitude of overpotential will decrease with temperature under the galvanostatic charging condition.

For the results of the potentiostatic charging shown in Fig. 3, we find that the magnitude of $\partial n_H/\partial T$ is less than the equilibrium and galvanostatic cases, i.e. $\partial n_H/\partial T$ changes from -1×10^{-3} K^{-1} to -7.4×10^{-4} K^{-1}, while the her changes from the equilibrium to the coupled Volmer–slow Tafel mechanism, as indicated by Eqs. (28), (38) and (49). At the same time, $\partial\log(-j)/\partial(1/T)$ shown in Fig. 3(b) changes from -1.4×10^3 K to -2.1×10^3 K, as indicated by Eqs. (40) and (51). The slopes change more gently in Fig. 3(b) than in Fig. 2(b).

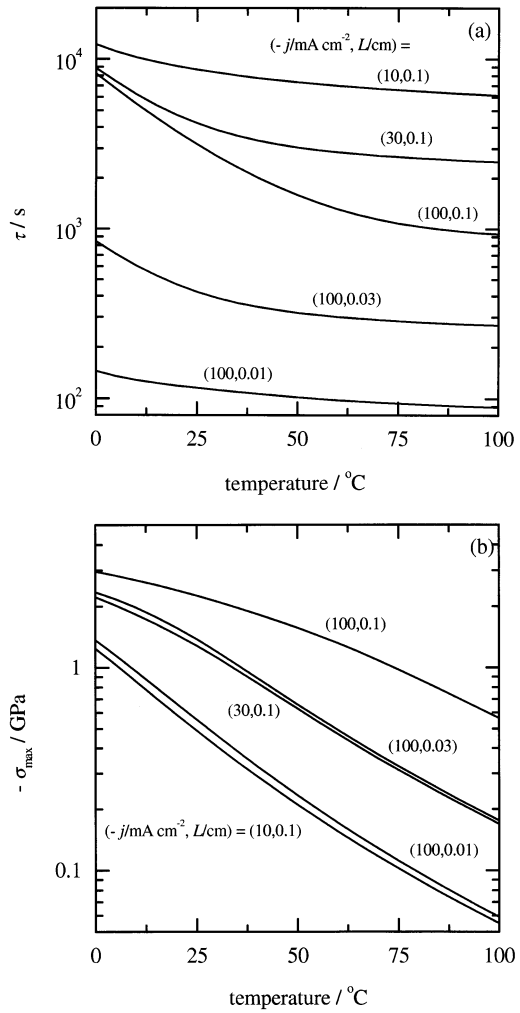

Fig. 4. Effects of temperature on (a) the half absorption time τ and (b) the maximum self-stress under galvanostatic charging conditions. The current density and plate thickness are shown beside each curve, the initial condition is the equilibrium state, the other parameters are the same as those of Fig. 2.

The change of n_H with T has two origins: one is the thermodynamic contribution as the isobar shown in Fig. 2(a) or indicated by Eq. (28) and the same term appeared in Eqs. (34), (38), (45) and (49); another is caused by the kinetic process. By comparing Eqs. (34) and (45) with Eqs. (38) and (49), we find that the kinetic process contributes to $\partial n_H/\partial T$ negative and positive terms under galvanostatic and potentiostatic charging conditions, respectively. This can explain the difference between $\partial n_H/\partial T$ under these two conditions. A crude but intuitive explanation can be used to understand this difference. Because n_H is determined by the relative cd, j/j_{0T} [13], or overpotential [11], so changes in j/j_{0T} and η reflect the change in n_H in some way. For galvanostatic charging, the exchange cd j_{0T} increases with T; this makes j/j_{0T} decreases with T, hence n_H decreases somewhat more rapidly than in the equilibrium case. For potentiostatic charging, the constant overpotential ensures that the chemical potential of H in Pd changes more slightly with T, so n_H changes less with T than in other cases.

By comparison of our theory with the experimental results given in Ref. [5], we find that $\partial n_H/\partial T \sim -1.6 \times 10^{-3}$ K^{-1} under the galvanostatic charging condition and $\partial n_H/\partial T \sim -8.7 \times 10^{-4}$ K^{-1} under the potentiostatic charging condition lie in the corresponding range of our results shown in Figs. 2(a) and 3(a), respectively, although the relevant experimental parameters are not available. Also, the fact that n_H decreases more rapidly in galvanostatic charging than in potentiostatic charging supports other aspects of our theory.

3.3. Hydrogen absorption rate

The temperature affects the absorption rate as well as the loading ratio [1]. To characterise this quantitatively, we introduce the absorption ratio:

$$M(t) = \frac{\bar{n}_H(t) - n_{H,0}}{n_{H,\infty} - n_{H,0}} \tag{52}$$

with $\bar{n}_H(t)$ and $n_{H,\infty}$ being the average and saturation values of n_H, respectively. We define the half absorption time τ at which $M(\tau) = 1/2$; the value of τ reflects the mechanism of the absorption process [13,14]. We calculate and show τ at different plate thicknesses and temperatures under galvanostatic and potentiostatic charging conditions in Figs. 4(a) and 5(a), respectively. For the galvanostatic charging situation shown in Fig. 4(a), we find that a higher temperature results in a lower τ value and hence higher absorption efficiency, as was verified experimentally [1], and τ approaches a saturation value if T is large enough. This means that H diffusion in the electrode is so fast that the interface reaction becomes the rate determining step when the temperature is high, so τ approaches an asymptotic value. When the plate thickness is small and/or the cd is low, a relatively low temperature is sufficient to ensure this mechanism, as discussed earlier [13]. In contrast, it needs a relatively high temperature to reach the same mechanism when L and/or j are large.

For potentiostatic charging (Fig. 5(a)), we find the behavior of τ changes with temperature and the plate thickness is the same as that of the concentration step diffusion, i.e. $\tau \propto L^2$ and $\tau \propto 1/D \propto \exp(U_D/T)$. This means that the bulk process determines the kinetics of hydrogen absorption. The small differences in τ between different overpotential values with the same plate thickness are caused mainly by different values of the concentration step.

In the conventional treatment of hydrogen charging into a electrode, the potentiostatic charging is approximated by H diffusion in the electrode with the boundary condition of the concentration steps; and the galvanostatic charging is considered as a diffusion

problem with the boundary condition of constant flux. Our results indicate that the former approximation is effective because the penetration reaction is under pseudo-equilibrium, but the validity of the latter assumption depends on the temperature in addition to the cd and plate thickness [13].

3.4. Self-induced stress

Earlier works revealed that hydrogen diffusion in Pd will induce a stress, and it alters the kinetic process and destroys the lattice when its magnitude exceeds the yield stress of the sample [14,35–37]. On the basis of Eqs. (1)–(10), we calculate the stress developed in samples with various thicknesses and show the maximum stresses as a function of temperature in Fig. 4(b) for the galvanostatic charging and Fig. 5(b) for the potentiostatic charging. For galvanostatic charging, it was found that an increase of temperature suppresses the stress especially when values of L and/or j are small; this means that a high temperature is in favour of the preservation of the original state of the sample. The reason is that H diffusion becomes the fast step and the H concentration inhomogeneity decreases, so the maximum stress decreases correspondingly. On the other hand, the maximum stress changes slightly with T, while the plate thickness and/or cd are large.

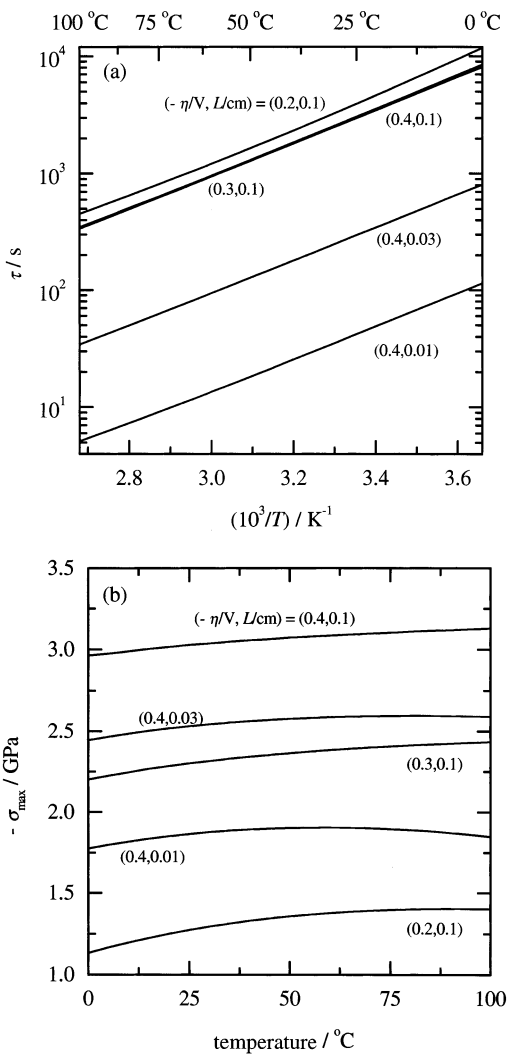

Fig. 5. Effects of temperature on (a) the half absorption time τ and (b) the maximum self-stress under potentiostatic charging conditions. The overpotential and plate thickness are shown beside each curve, the initial condition is the equilibrium state, the other parameters are the same as those of Fig. 2.

For potentiostatic charging the hydrogen absorption is controlled by H diffusion in Pd bulk and the maximum stress is determined by the H concentration step, as discussed by Li [25], therefore, the maximum stress changes slightly with temperature, as shown in Fig. 5(b).

In this paper, we discuss only the situation of hydrogen absorption symmetrically into Pd electrodes and do not discuss the unsymmetrical absorption, as was done in an earlier paper [14]. This is because the symmetrical absorption will induce larger stresses than in the unsymmetrical case, so the discussion about the former is sufficient to illustrate the effects of temperature on the stress.

In practice, Young's modulus decreases with temperature. Consequently, the induced self-stresses are less than deduced in the present work, but the corresponding half absorption time τ is somewhat longer than in the present work [14].

4. Discussion

In this paper, we discuss specifically the situation of the her in the acidic solution; there is a change in the her mechanism from the fast Volmer–slow Tafel type to the coupled Volmer–Tafel type with increasing cd (or overpotential). But for basic solutions, the valid cd range for the fast Volmer–slow Tafel mechanism is very narrow and even disappears; otherwise, the coupled Volmer–Tafel mechanism dominates the her in a wide cd range due to the small value of j_{0V}/j_{0T} and a large heterogeneity energy U_s [11,32]. Our method and results can be applied to this situation with some parameters modified. On the other hand, additives and Pd alloy electrodes are always used to improve the electrode performance for H absorption in experiments. Their effects can be expressed by the same formulae with some parameters also adjusted.

Because all of the symmetry factors and the transfer coefficient in Eqs. (1)–(3) are chosen to be 1/2 and all of the enthalpies and entropies do not change with temperature, our results have a simple but ideal form, i.e. the changes of n_H, η and j with T are expressed in terms of four quantities $\Delta H_{gb} + U_b n_H$, ΔH_{gs}, U_{0V} and

U_{0T} besides the other usual parameters, although many factors are involved. If non-ideal contributions of the symmetric factor, transfer coefficient, enthalpy and entropy etc. are concerned, a higher order approximation is necessary but the analytical form may be more complicated than that derived here.

In the paper, we discuss mainly the loading ratio change with j (or E) under the galvanostatic (or potentiostatic) charging condition. However, our theory can be applied to the problem of maintaining the loading ratio by increasing the amplitude of j or E at high temperature. The solution is directly given by Eqs. (31), (33), (42) and (44).

It must be pointed out that our theory is more phenomenological than fundamental. A general treatment should be based on the absolute rate theory considering subtle effects of temperature on all aspects of the Pd|H electrode process, e.g. the temperature dependence of solute activity, the activation energy of each step and other related issues. It needs more experiment details also. However, our results give the primary effects and there is some experimental evidence supporting our conclusions. Although a systematic experimental study on this subject has not been done up to now, we hope our work can stimulate further research on this issue.

5. Conclusions

On the basis of thermokinetics of the Pd|H electrode, which includes various steps in the hydrogen evolution reaction, diffusion and self-stress of H in Pd, we have discussed the temperature effects on various aspects of the hydrogen absorption. Our results indicate that the loading ratio decreases with increasing temperature for both galvanostatic and potentiostatic charging conditions, and its amplitude depends on the charging pattern, and the chemical and electrochemical parameters of the Pd|H electrode. We have found that the increase in temperature accelerates hydrogen absorption into palladium for both galvanostatic and potentiostatic charging conditions. The self-stress decreases with increasing temperature for galvanostatic charging, but it changes slightly for potentiostatic charging. Finally, our theory fits the available experimental results.

6. List of symbols

A_i Arrhenius frequency factor of rate constant for reaction i
a_i activity of substance i dissolved in the electrolyte solution
D diffuison coefficient of H in Pd, $cm^2\ s^{-1}$
E electrode potential, V
E_0 reversible electrode potential, V
F Faraday constant, 96484.56 C mol^{-1}
f_{H_2} fugacity of H_2 gas, atm
$\Delta\bar{H}_{ij}$ hydrogen enthalpy change from ideal state i to ideal state j, J mol^{-1}
j current density, mA cm^{-2}
j_i current density of reaction i, mA cm^{-2}
j_{0i} exchange current density of reaction i, mA cm^{-2}
L plate thickness, cm
M H absorption ratio
n_H H/Pd atomic ratio
$n_{H,0}$ initial value of n_H, it is the same as the equilibrium value of n_H in the paper
$n_{H,\infty}$ saturation value of n_H in the absorption process
$\bar{n}_H(t)$ average value of n_H at time t
R universal gas constant, 8.314 J mol^{-1} K^{-1}
r surface roughness factor
ΔS_{ij} hydrogen entropy change from ideal state i to ideal state j, J mol^{-1} K^{-1}
T absolute temperature, K
t time, s
U_b non-ideal interaction energy of H in the bulk of β-PdH_x, 44.9 kJ mol^{-1} for both H and D
U_i activation energy of reaction i, J mol^{-1}
U_{0i} apparent activation energy of j_{0i}, J mol^{-1}
U_s heterogeneity energy of the Frumkin adsorption, J mol^{-1}
V_H partial molar volume of H in β-PdH_x, 1.55 cm^3 mol^{-1}
v_C reaction rate of H_2 congregation reaction, mol s^{-1}
Y Young's modulus, Pa
z coordinate along the thickness direction, cm

Greek symbols

β_V transfer coefficient of the Volmer reaction
Γ_b maximum molar number of available sites for H per unit volume of PdH_x, 0.10 mol cm^{-3}
Γ_s maximum H molar number of available sites per real unit area, 2.20×10^{-9} mol cm^{-2}
η overpotential, V
ν Poisson's ratio
θ fractional surface coverage of H on Pd
θ_o value of θ in equilibrium
σ self-stress caused by hydrogen inhomogeneity distribution in Pd, Pa
σ_{max} maximum value of σ, Pa
τ half absorption time, s

Subscripts

b	state of hydrogen in Pd bulk
C	congregation reaction
D	H diffusion
g	state of hydrogen in H_2 gas
i	state of hydrogen in ionic state
O	H_3^+O in acidic solution and at low negative overpotential, or H_2O in basic solution or at high negative overpotential
P	penetration reaction
R	H_2O in acidic solution and at low negative overpotential, or OH^- in basic solution or at high negative overpotential
s	state of hydrogen adsorption on Pd surface
T	Tafel reaction
V	Volmer reaction
0	equilibrium state
+	anodic reaction
−	cathodic reaction

Acknowledgements

The work was supported by the Natural Science Foundation of China, Pan-Deng Project of the Department of Science and Technology of China under Grant No. 95-yu-41 and the Foundation of China Academy of Engineering Physics.

References

[1] A.M. Riley, J.D. Seader, D.W. Pershing, C. Walling, J. Electrochem. Soc. 139 (1992) 1342.
[2] V. Kapali, M. Ganesan, M.A. Kulandainathan, A.S. Mideen, K.B. Sarangapani, V. Balaramachandran, S.V. Iyer, B. Muthuramalingam, J. Electroanal. Chem. 364 (1994) 95.
[3] G. Mengoli, M. Fabrizio, C. Manduchi, E. Milli, G. Zannoni, J. Electroanal. Chem. 390 (1995) 135.
[4] A. Wark, S. Crouch-Baker, M.C.H. McKubre, F.L. Tanzella, J. Electroanal. Chem. 418 (1996) 199.
[5] M. Bernardini, N. Comisso, M. Fabrizio, G. Mengoli, A. Randi, J. Electroanal. Chem. 453 (1998) 221.
[6] M. Enyo, P.C. Biswas, J. Electroanal. Chem. 335 (1992) 309.
[7] T. Green, D. Britz, J. Electroanal. Chem. 412 (1996) 59.
[8] G. Muto, H. Yoshitake, N. Kamiya, K.I. Ota, J. Electroanal. Chem. 457 (1998) 99.
[9] F.A. Lewis, The Palladium Hydrogen System, Academic Press, London, 1967, p. 47.
[10] E. Wicke, H. Brodowsky, Hydrogen in palladium and palladium alloys, in: G. Alefeld, J. Völkl (Eds.), Hydrogen in Metals II, Application Oriented Properties, Topics in Applied Physics, vol. 29, Springer, Berlin, 1978, p. 73.
[11] M. Enyo, Hydrogen electrode reaction on electrocatalytically active metals, in: B.E. Conway, J.O'M Bockris, E. Yeager, S.U.M. Khan, R.E. White (Eds.), Kinetics and Mechanism of Electrode Processes, vol. 7, Plenum, New York, 1983, p. 241.
[12] W.S. Zhang, X.W. Zhang, H.Q. Li, J. Electroanal. Chem. 434 (1997) 31.
[13] W.S. Zhang, Z.L. Zhang, X.W. Zhang, F. Wu, J. Electroanal. Chem. 474 (1999) 123.
[14] W.S. Zhang, Z.L. Zhang, X.W. Zhang, J. Electroanal. Chem. 474 (1999) 130.
[15] E. Wicke, G.H. Nernst, Ber. Bunsenges. Phys. Chem. 68 (1964) 224.
[16] Y. Sakamoto, M. Imoto, K. Takai, T. Yanaru, K. Ohshima, J. Phys.: Condens. Mater. 8 (1996) 3229.
[17] J.E. Schirber, B. Morosion, Phys. Rev. B 12 (1975) 117.
[18] R. Felici, L. Bertalot, A. De Ninno, A. La Barbera, V. Violante, Rev. Sci. Instrum. 66 (1995) 3344.
[19] B. Baranowski, S. Majchrzak, T.B. Flanagan, J. Phys. F: Met. Phys. 1 (1971) 258.
[20] R. Woods, Chemisorption at electrodes, in: A.J. Bard (Ed.), Electroanalytical Chemistry: A Series of Advances, vol. 9, Marcel Dekker, New York, 1976, p. 1.
[21] M. Enyo, J. Electroanal. Chem. 134 (1982) 75.
[22] O. Savadogo, K. Amuzgar, D.L. Piron, Int. J. Hydrog. Energy 15 (1990) 783.
[23] F.J. Millero, Effects of pressure and temperature on activity coefficients, in: P.M. Pytkowicz (Ed.), Activity Coefficients in Electrolyte Solutions, vol. 2, CRC Press, Boca Raton, FL, 1979, p. 63.
[24] A.L. Horvath, Handbook of Aqueous Electrolyte Solutions: Physical Properties, Estimation, and Correlation Methods, Ellis Horwood Series in Physical Chemistry, Wiley, New York, 1985, p. 206.
[25] J.C.M. Li, Metall. Trans. A 9 (1978) 1353.
[26] F.C. Larché, J.W. Chan, Acta Metall. 30 (1982) 1835.
[27] A. De Ninno, V. Violante, A. La Barbera, Phys. Rev. B 56 (1997) 2417.
[28] S. Majorowski, B. Baranowski, J. Phys. Chem. Solids 43 (1982) 1119.
[29] S. Majorowski, B. Baranowski, in: P. Jean, C.H. Satterthwaite (Eds.), Electronic Structure and Properties of Hydrogen in Metals, Plenum, New York, 1983, p. 519.
[30] J. Crank, The Mathematics of Diffusion, Clarendon, Oxford, 1975, p. 3.
[31] E. Gileadi, Electrode Kinetics for Chemists, Chemical Engineers, and Material Scientists, VCH, New York, 1993, p. 261.
[32] J.H. Chun, K.H. Ra, J. Electrochem. Soc. 145 (1998) 3794.
[33] W.S. Zhang, X.W. Zhang, X.G. Zhao, J. Electroanal. Chem. 458 (1998) 107.
[34] P.K. Subramanyan, Electrochemical aspects of hydrogen in metals, in: J.O'M. Bockris, B.E. Conway, E. Yeager, R.E. White (Eds.), Comprehensive Treaties of Electrochemistry, vol. 4, Plenum, New York, 1981, p. 411.
[35] F.A. Lewis, J.P. Magennis, S.G. McKee, P.J.M. Seebuwufu, Nature 306 (1983) 673.
[36] Y. Sakamoto, H. Tanaka, F.A. Lewis, X.Q. Tong, K. Kandasamy, Int. J. Hydrog. Energy 21 (1996) 1025.
[37] X.Q. Tong, Y. Sakamoto, F.A. Lewis, R.V. Bucur, K. Kandasamy, Int. J. Hydrog. Energy 22 (1997) 141.